Photoelectrochemical behavior of phthalocyanine-sensitized TiO_2 in the presence of electron-shuttling mediators

Photoelectrochemical behavior of phthalocyanine-sensitized TiO_2 in the presence of electron-shuttling mediators

Shahid Ullah Khan[1,2,3], Stanislav Trashin[1,2], Victoria Beltran[1,2], Yuliya S. Korostei[4], Marius Pelmus[5], Sergiu M. Gorun[5], Tatiana V. Dubinina[4,6], Sammy W. Verbruggen[2,3] and Karolien De Wael[1,2,*]

[1]A-Sense Lab, Department of Bioscience Engineering, University of Antwerp, 2020 Antwerp, Belgium; [2]NANOlab Center of Excellence, University of Antwerp, 2020 Antwerp, Belgium; [3]DuEL Research Group, Department of Bioscience Engineering, University of Antwerp, 2020 Antwerp, Belgium; [4]Instituite of Physiologically Active Compounds, Russian Academy of Science, 14243 Chernogolovka, Moscow Region, Russian Federation; [5]Department of Chemistry and Biochemistry and the Centre for Functional Materials, Seton Hall University, New Jersey, 07079, USA; [6]Department of Chemistry, Lomonosov Moscow State University, 119991 Moscow, Russian Federation

[*]Corresponding author: karolien.dewael@uantwerpen.be

ABSTRACT: Dye-sensitized TiO_2 has found many applications for dye-sensitized solar cells (DSSC), solar-to-chemical energy conversion, water/air purification systems, and (electro)chemical sensors. We report an electrochemical system for testing dye-sensitized materials that can be utilized in photoelectrochemical (PEC) sensors and energy conversion. Unlike related systems, the reported system does not require a direct electron transfer from semiconductors to electrodes. Rather, it relies on electron-shuttling by redox mediators. A range of model photocatalytic materials were prepared using three different TiO_2 materials (P25, P90, and PC500) and three sterically hindered phthalocyanines (Pcs) with electron-rich *tert*-butyl substituents (*t*-Bu_4PcZn, *t*-Bu_4PcAlCl, and *t*-Bu_4PcH_2). The materials were compared with previously developed TiO_2 modified by electron-deficient, also sterically hindered fluorinated phthalocyanine F_{64}PcZn, a singlet oxygen ($^1O_2$) producer, as well as its metal-free derivative, $F_{64}PcH_2$. The PEC activity depended on the redox mediator, as well as type of TiO_2 and Pc. By comparing the responses of one-electron shuttles, such as $K_4Fe(CN)_4$, and $^1O_2$-reactive electron-shuttles, such as phenol, it is possible to distinguish the action mechanism of the supported photosensitizers, while the overall activity can be assessed using hydroquinone. *t*-Bu_4PcAlCl showed significantly lower blank responses and higher specific responses towards chlorophenols compared to *t*-Bu_4PcZn due to the electron-withdrawing effect of Al^{3+} metal center. The combination of reactivity insights and the need for only μg amounts of sensing materials renders the reported system advantageous for practical applications.

INTRODUCTION

Photocatalytically and photoelectrochemically active materials, such as dye-sensitized semiconductors have found utility for environmental remediation[1-3], solar-to-chemical energy conversion[4, 5], (bio)sensors[6, 7], and dye-sensitized solar cells.[8, 9] Photoelectrochemical (PEC) devices and materials are of particular interest for sensors.[10, 11] The separation of excitation sources (optics) and detection modus operandi (electrochemistry) improves the performances of PEC devices as sensors[12, 13], leading to faster responses, higher sensitivity, and the elimination of undesired backgrounds.[14-16]

Efficient PEC materials exhibit special structural and energetic features. Thus, materials such as nanostructured semiconducting oxides[17, 18], carbon-based materials[19], and metal nanoparticles[20] have been exploited for PEC analysis. Titanium dioxide, TiO_2, is, arguably, the benchmark photocatalyst due to its nontoxic nature, photochemical stability, and low cost.[21, 22] However, the photoactive anatase TiO_2 has a 3.2 eV wide bandgap, limiting its photocatalytic activity to the UV region.[23] Approaches to extend TiO_2 absorption to the visible region include doping[21, 23] and deposition of Vis-NIR absorbing photosensitizers (PSs) on its surface.[24, 25]

Phthalocyanines (Pcs) are extensively conjugated macrocycles structurally related to chlorophyll and porphines, Fig. 1. Their extensive conjugation ensures a narrow HOMO-LUMO gap, consequently absorbing light in the visible region of the electromagnetic spectrum. Pcs have been widely used as PSs due to their high extinction coefficients, superior thermal and chemical stability, high quantum yields for triplet state formation, and $^1O_2$ generation.[26-28] Furthermore, the compositional and structural versatility of Pcs allows tuning their chemical and photophysical properties, particularly for enhancing their chemical robustness and introducing functional groups that, for example, may serve to anchor Pcs on various surfaces.[29, 30]

Most of the previously reported PEC sensors rely on a photoinduced electron transfer from a PS to a semiconductor, followed by an electron transfer from the semiconductor to an electrode, Fig. 2A.[31-34] The electrode, in this case, is polarized accordingly to play a role of the electron acceptor (anode). We have recently reported a different PEC sensing approach, namely the use of a PS to generate analyte-oxidizing singlet oxygen, $^1O_2$, Fig. 2B.[6, 11, 30, 35] The used PS, F_{64}PcZn, Fig. 1D, contains bulky, perfluorinated iso-propyl peripheral substituents

that ensure it remains a single-site catalyst both in solution and solid-state films and resists the destructive action of $^1O_2$ and its daughter radicals.[36] Notably, the supporting TiO_2 semiconductor is not subject to electron injection from the photoexcited $F_{64}PcZn$ due to the electron-withdrawing effect of fluorine substituents that stabilize the LUMO by more than 1 eV[37] relative to PcZn, Fig 1C. Thus, in the presence of TiO_2, the visible-light photogenerated $^1O_2$ is the main reactive species for the chemical conversion of analytes such as hydroquinone or phenol, playing the role of redox mediators. The subsequent electrochemical reduction of oxidized (oxygenated) analytes at the cathode creates an electrochemical reduction-photocatalytic oxidation redox cycle, thus enhancing the obtained steady-state photocurrent response.[6]

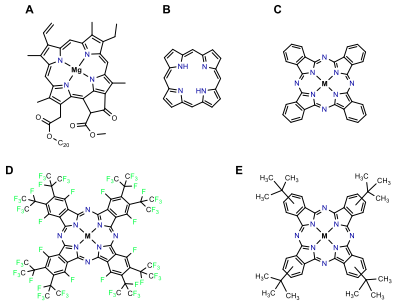

Figure 1. Selected natural and related, synthetic macrocycles that absorb light in the visible region: chlorophyll (A), porphine (B), unsubstituted zinc phthalocyanine M = Zn (C), fluoroalkyl phthalocyanine $F_{64}PcM$, M = Zn, 2H (D), alkyl phthalocyanine *t*-Bu_4PcM, M = Zn, AlCl, 2H (E).

Here we report the preparation and properties of semiconducting TiO_2 composites containing electron-rich phthalocyanines namely *t*-Bu_4PcZn, *t*-$Bu_4PcAlCl$, and *t*-Bu_4PcH_2, Fig. 1E. Unlike the electron-withdrawing, bulky iso-perfluoropropyl groups, the electron releasing *tert*-butyl groups facilitate the injection of an electron from the photoexcited PS into the CB of TiO_2. However, a few μm thick layer of powdered TiO_2 does not provide an interface for an efficient electron transfer from TiO_2 to an underlying electrode, especially in the presence of O_2 as an alternative electron acceptor. Therefore, we put forward the new PEC detection mechanism (Fig. 2C), based on the redox shuttling not involving $^1O_2$ formation. The photoexcited PS injects an electron into the CB of TiO_2 which is electrically disconnected from an electrode. The analyte (A) shuttles electrons from an electrode to the PS, restoring its initial redox state (Fig. 2C).

Previously, Bard and co-workers[31] studied a PEC system based on unsubstituted phthalocyanines, Fig. 1C, and TiO_2 single crystals in electrical contact with an In-Ga alloy, Fig. 2A. Those measurements were conducted under an N_2 atmosphere to exclude scavenging of electrons from the CB of TiO_2 by O_2. In contrast, the photocurrent in our system is measured under ambient conditions and using powder PS-TiO_2 drop-casted from water suspension on screen-printed electrodes. Instead of direct electron transfer, the PEC responses in our system result from the conversion of redox species freely diffusing in the near-electrode layer, Fig. 2C. The use of the electron-shuttling mechanism to probe the reactivity of bulk Pc-TiO_2 materials and detect analytes capable of the reversible redox cycling is reported here for the first time.

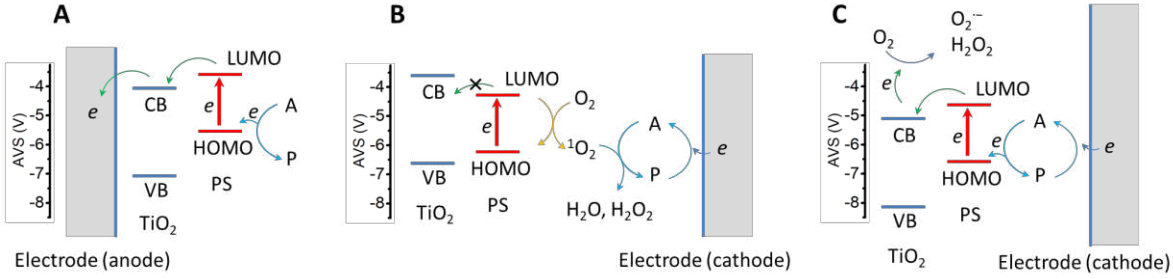

Figure 2. PEC detection of an analyte based on (A) the direct electron transfer from PS to the conduction band (CB) of TiO_2 and then to a polarized electrode, (B) photosensitized formation of $^1O_2$, (C) and the electron shuttling without $^1O_2$ formation.

EXPERIMENTAL

Materials. Zinc 2, 9, 16, 23-tetra-*tert*-butyl-phthalocyanine (*t*-Bu_4PcZn, Mr = 802, purity 95%), 2, 9, 16, 23-tetra-*tert*-butyl-29H, 31H-phthalocyanine (*t*-Bu_4PcH_2, Mr = 739, purity 97%), Zinc phthalocyanine (PcZn, Mr = 578, purity 97%) were purchased from Sigma-Aldrich (Belgium). Aluminum tetra-*tert*-butylphthalocyanine, *t*-$Bu_4PcAlCl$ (*t*-$Bu_4PcAlCl$, Mr = 799),[39] the perfluorinated phthalocyanine zinc complex ($F_{64}PcZn$, Mr = 2066)[40] and its metal-free analog ($F_{64}PcH_2$, Mr = 2003)[41, 42], were synthesized as previously described. The chemical structures of the Pcs used in this study are shown in Fig. 1C-E. Hydroquinone (HQ, 99.5%) was purchased from Acros Organics, Belgium. Methanol (CH_3OH, 99.8% HPLC grade) was purchased from Fisher Chemical. KH_2PO_4 and KCl were purchased from Sigma-Aldrich (Belgium). Ultrapure MQ water was used for all experiments. Titanium dioxide (TiO_2), Aeroxide P25 and Aeroxide P90 were obtained from Evonik Inorganic Materials (USA). TiO_2 PC500 was obtained from CristalActiV. Amoxicillin trihydrate of purity >98.0% and oxytetracycline hydrochloride of purity >95.0% were obtained from TCI Europe (Belgium). Cefadroxil of purity > 99.0% was obtained from Acros-Organics and tetracycline of purity 98.0–102.0% was obtained from Sigma-Aldrich (Belgium). Other phenolic compounds were of 98% purity or better and were obtained from different suppliers. L-Ascorbic acid of 99.5% purity was obtained from Sigma-Aldrich (Belgium). The solid-state properties of the TiO_2 supports are given in Table S1. Nitrogen adsorption-desorption isotherms were measured using a 3P Meso 112 instrument. All samples were degassed overnight at 100 °C prior to use. The specific surface area was calculated from nitrogen adsorption isotherms by the Brunauer-Emmett-Teller (BET) method. The pore size distribution and pore volume were calculated by the Brunauer-Joyner-Halenda (BJH) method. Contact angle measurements were carried out with an Ossila

sessile drop-based contact angle goniometer equipped with a high-resolution camera (1920 x 1080). The volume of the droplet used was 4 µL.

Pcs-supported TiO_2 (Pcs∪TiO_2) modified electrodes. The Pcs were dissolved in an appropriate solvent (*t*-Bu_4PcAlCl and *t*-Bu_4PcZn in isopropanol, *t*-$BuPcH_2$ in THF, F_{64}PcZn and $F_{64}PcH_2$ in ethanol) to reach 1 mg/mL (1.3-1.5 mM for *t*-Bu_4Pcs and 0.5 mM for F_{64}Pcs). Next, 10 mg TiO_2 was added in 0.33 mL of each solution, and the solvents were evaporated at 60°C using a thermal shaker (Thermo Scientific). Then 1 mL of MQ water was added to the dried powders, vortexed, and sonicated until a milk-like homogenous suspension of 10 mg/mL Pcs∪$TiO_2$was obtained. The immobilization procedure yields 3 wt% loading of Pcs, confirmed spectrophotometrically by back leaching the Pcs with organic solvents. Other loadings for *t*-Bu_4PcAlCl/Zn/2H were prepared similarly using more diluted or more concentrated Pcs solutions. $F_{64}PcH_2$∪TiO_2 3 wt% was also prepared from a more diluted 0.03 mg/mL (0.015 mM) solution in EtOH to ensure complete disaggregation of the complex. Before modification, carbon screen-printed electrodes (ItalSens IS-C, working electrode Ø = 3 mm, obtained from PalmSens, the Netherlands) were first pre-wetted by dropping 1-2 µl 20% ethanol on the working electrode surface. Next, a 5 µL droplet of the 10 mg/mL Pcs∪TiO_2 water suspension was placed on the working electrode and dried in the dark, in a Petri dish containing silica gel desiccant.

Equipment

Electrochemical measurements. Electrochemical measurements were carried out using an Autolab Potentiostat/Galvanostat PGSTAT 302N from Metrohm (Utrecht, The Netherlands), operated with the NOVA 1.11 software. A diode laser emitting at 659 nm (Roithner Lasertechnik, Austria) was adjusted to 30 mW by using a light power meter (Thorlabs). The distance between the laser was set such that the beam entirely covered the working electrode. An Arduino Uno was programmed to switch on and off the light at given time intervals. All electrochemical measurements were performed in a droplet of 80 µL buffer solution (phosphate buffer pH 7) containing 0.1 M KCl and 0.02 M KH_2PO_4 dissolved in ultrapure water. All measurements were conducted first in pure buffer until a stable signal and then in the presence of an electron shuttle such as 100 µM HQ.

Electronic and Vibrational Spectroscopy. A UV-vis AvaSpec-2048L (Avantes) equipped with AvaLight-DH-S-BAL light source was used to record the optical properties of the Pcs. A UV-vis diffuse reflectance (UV-vis-DR) spectrophotometer UV-2600 (Shimadzu) equipped with an integrating sphere was used to record spectra of Pcs∪TiO_2 hybrid materials, referenced to $BaSO_4$. Transmission FTIR spectra were collected in the 4000 and 400 cm^{-1} range using a Bruker Alpha II machine with a DTGS detector. Measurements were conducted using KBr pellets (Sigma Aldrich, FTIR grade, ref. 221864). For each sample, 128 scans were accumulated with a resolution of 4 cm^{-1}.

RESULTS AND DISCUSSION

Electronic and vibrational spectroscopy of modified TiO_2 materials. Pcs exhibit in solution a narrow absorbance band in the red region (Q band). The Q band position, measured in solution at similar absorbance maxima, can vary significantly as a function of Pc substituents.[43] For Pcs immobilized on all TiO_2 supports, UV-vis-DR shows broad peaks in the 500 – 800 nm region, Fig. 3, of insufficient resolution to detect Pc-dependent Q-bands position shifts. For the tested Pcs, immobilization results in the broadening and 10-20 nm redshift of Q-bands, Fig. 3. A new absorbance shoulder at >750 nm appears. The changes correspond to the behavior of Pcs in solid-state films and have been ascribed to molecular distortions and intermolecular interactions through stacking and aggregation.[44-46] These interactions and aggregations are of concern for PEC measurements due to possible energy dissipation in photoexcited singlet and triplet states,[47] typically leading to decreased quantum yields and PEC responses, as demonstrated previously for a partially aggregated Al phthalocyanine and its stable dimer.[48]

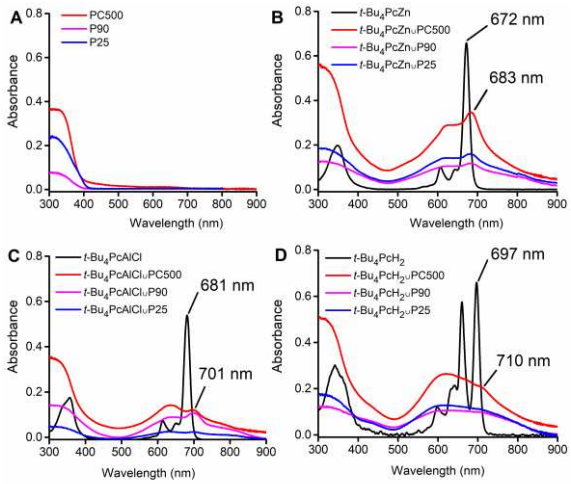

Figure 3. UV-vis-DR spectra of the utilized unmodified TiO_2 supports (A); UV-Vis spectrum in solution in comparison with UV-vis-DR spectra of deposited *t*-Bu_4PcZn (B), *t*-Bu_4PcAlCl (C), and *t*-Bu_4PcH_2 (D). *t*-Bu_4PcZn/AlCl were dissolved in methanol, *t*-Bu_4PcH_2 in THF.

FTIR spectra of both unmodified and modified TiO_2 are dominated by three major absorbance bands attributed to Ti-O stretching (νTi-O, 600 cm^{-1}), H-O-H deformation (δO-H, 1630 cm^{-1}), and a broad O-H stretching band associated with water, hydroxyl, and hydrogen bonds (νO-H, ca. 3400 cm^{-1}). When spectra of pure TiO_2 materials are referenced to Ti-O stretching band centered at 600 cm^{-1}, Fig. 4A, two other bands, related to water, increase proportionally with the specific TiO_2 surface area in order P25 < P90 < PC500. This trend mirrors the well-documented TiO_2 surface propensity to interact with moisture from air, leading to a layer of water adsorbed over the surface and dissociated to some extent.[49]

It is commonly known that a metal center in Pcs can interact with TiO_2 and other metal oxide surfaces due to axial coordination with adsorbed OH groups and water. Metal-free *t*-Bu_4PcH_2 does not have such an anchoring point and should adsorb weaker on metal oxide surfaces compared to *t*-Bu_4PcZn/AlCl, which is consistent with lower mobility of *t*-Bu_4PcAlCl/Zn compared to *t*-Bu_4PcH_2 on TLC plates, Fig. S1. Interestingly, FTIR spectra *t*-Bu_4PcH_2∪TiO_2 PC500 show a significant decrease in the region of hydrogen bonds (maximum at 3400 cm^{-1}) compared to *t*-Bu_4PcAlCl∪TiO_2 and *t*-$Bu_4PcZnTiO_2$, Fig. 4B, when the spectra are referenced to the deformation band of

water (1630 cm^{-1}). The difference is even more pronounced for TiO_2 P25 and P90 (Fig. S2). This observation suggests that, compared to *t*-Bu_4PcH_2 a higher number of hydrogen bonds and OH-groups may form after the immobilization of *t*-$Bu_4PcAlCl$ and *t*-Bu_4PcZn. FTIR spectra of pure *t*-$Bu_4PcAlCl$ and *t*-Bu_4PcZn also show an increased 3400 cm^{-1} band, Fig. S3, while this band is minimal in the case of *t*-Bu_4PcH_2. This is reasonable considering the lack of metal where water could coordinate. Moreover, the FTIR spectrum of *t*-$Bu_4PcAlCl$ (Fig. S3) shows a characteristic band at 3220 cm^{-1} attributed to stretching of hydroxyl groups. The band is lower in *t*-Bu_4PcZn and not detected in *t*-Bu_4PcH_2 in contrast to the characteristic N-H stretching band in *t*-Bu_4PcH_2 at 3292 cm^{-1}. The increased bands at 3220 and 3400 cm^{-1} in *t*-$Bu_4PcAlCl$ show that Cl in *t*-$Bu_4PcAlCl$ does not prevent the interaction of Al^{3+} with water, as per its known lability.[50]

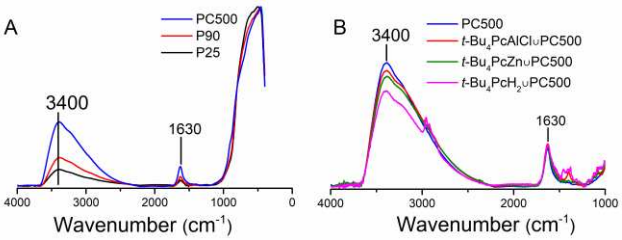

Figure 4. FTIR spectra of (A) bare TiO_2 PC500, P90, and P25 after calibration based on the Ti-O stretching band at 600 cm^{-1}; (B) TiO_2 PC500 unmodified and modified by *t*-Bu_4PcZn/AlCl/2H after calibration using the water deformation band at 1630 cm^{-1}. The same trend is observed for TiO_2 P90 and P25 (Fig. S2).

Energy alignment of Pc molecular orbitals and TiO_2 bands. The relative energy position of the LUMO of Pcs and the CB of TiO_2 determines the possibility for electron injection from photoexcited Pcs into the CB of TiO_2. The absolute energy levels of LUMO can be determined from voltammetric data, namely from the first reduction potentials, using the formula AVS = $-E°'Red_1$(in V vs. SHE) − 4.5 V, where AVS corresponds to the energy in the absolute voltage scale and $E°'Red_1$ is the formal potential for the first reduction transition in Pcs. The formal potentials obtained in acetonitrile, Table S2 and Fig. S4, agree with previous reports on the electron-withdrawing effect of fluorine on formal potentials of the planar Zn phthalocyanine $H_{16}PcZn$ (Fig. 1C) and its fluorinated analog, $F_{16}PcZn$[51, 52], as well as with DFT calculations that predicted stronger stabilization of LUMO in $F_{64}PcZn$ compared to $F_{16}PcZn$.[37]

The first reduction potential of *t*-Bu_4PcZn (−0.761 V vs. SHE) and thus the LUMO (−3.74 V in AVS) are shifted by 0.91 V compared to the first reduction potential of $F_{64}PcZn$ (0.150 V vs. SHE) and its LUMO (−4.65 V in AVS). Thus, the LUMO in *t*-Bu_4PcZn lies above the CB of TiO_2 (−4.21 V in AVS) by 0.47 V, making the electron transfer from a photoexcited *t*-Bu_4PcZn to TiO_2 favorable. In contrast, the LUMO of $F_{64}PcZn$ lies below the CB of TiO_2 by 0.44 V, making such transfer unfavorable. Interestingly, binding Cl^- to Zn may shift the reduction potentials by about 0.3 V, Table S2. Nevertheless, even if Cl^- in the water phase binds to immobilized $F_{64}PcZn$, the potential should still stay below the CB of TiO_2. Fig. 2 shows the positions of the energy bands in alignment with the electrochemical data for $F_{64}PcZn$ and *t*-Bu_4PcZn in acetonitrile. The electrochemical HOMO-LUMO gaps are 1.6 – 1.7 V and correspond to the literature data for other phthalocyanines[39, 51, 52], the energy of the Q-band (hc/λonset) and previous DFT calculations.[37] In comparison to *t*-Bu_4PcZn, $E°'Red_1$ of *t*-Bu_4PcH_2 is by 0.23 V lower[53] (the LUMO is by 0.23 V higher) and $E°'Red_1$ of *t*-$Bu_4PcAlCl$ is by 0.28 V higher[39] (the LUMO is by 0.28 V lower) due to the effect of the central metal. Nevertheless, it does not change the general picture principally. All three *t*-Bu_4PcZn, *t*-$Bu_4PcAlCl$, and *t*-Bu_4PcH_2 should be able to transfer an electron from photoexcited PS to TiO_2 according to the mechanism depicted in Fig. 2C.

Confirmation of the reaction mechanism by PEC measurements. Fig. 5A-D shows the voltammetric behavior of four different electron donors. HQ and $K_4Fe(CN)_6$ demonstrate reversible redox transition at 0.028 V (0.312 V vs. SHE) and 0.160 V (0.444 V vs. SHE), respectively, Fig. 5A and C. Phenol, in addition to its irreversible oxidation at 0.57 V (0.85 V vs. SHE), Fig. 5B, also electropolymerizes at the electrode surface giving, in the next successive scans, a pair of broad waves around 0.2 V (0.48 V vs. SHE) that are also seen after washing the electrode and conducting the same voltammetric measurements in pure buffer, Fig. 5B. This behavior is driven by the formation of phenolic cation radicals.[54, 55] Its polymerization causes the electrode fouling expressed as a decrease in the phenol oxidation peak current and its shift towards higher potentials with cycle number. In contrast to others, ascorbic acid behaves fully irreversibly with a transition around 0.08 V (0.36 V vs. SHE), Fig. 5D, which is close to the potential of HQ.

Unlike phenol, HQ is oxidized reversibly to benzoquinone (BQ) via an electron transition process without obvious side reactions, Fig 5A. It is also known that HQ readily oxidizes into BQ by $^1O_2$[56-58], also noted in our previous studies with solubilized $^1O_2$ producing photosensitizers.[48] At potentials lower than 0 V, BQ is reduced back to HQ, as per the cyclic voltammogram shown in Fig. 5A. Thus, HQ can serve as an electron shuttle in both systems, viz. the electron transition and $^1O_2$ formation, Fig. 2B and C. Indeed, a high photocurrent is observed in the presence of HQ for electrodes modified with *t*-$Bu_4PcZn\cup TIO_2$, Fig. 5E, and $F_{64}PcZn\cup TiO_2$, Fig. 5I. The photocurrent is about 4x higher in the case of $F_{64}PcZn$, most probably due to faster reaction kinetics and efficient $^1O_2$ formation.

Importantly, phenol behaves differently in the reaction with $^1O_2$ and at the electron transition. Phenol is oxidized to BQ by $^1O_2$ via an endoperoxide formed as an intermediate by the [4+2]-cycloaddition of $^1O_2$ to its aromatic ring.[56-59] In contrast, phenol oxidation via electron transfer leads to a cation radical and subsequent oligomers, thus hindering the reversibility of the process. Accordingly, TiO_2 modified by *t*-Bu_4PcZn gives no significant photocurrent, Fig. 5F, whereas $F_{64}PcZn$ involving $^1O_2$ results in a strong photocurrent, Fig. 5J, which accounts for 20% of that in the presence of HQ.

A well-known one electron donor $K_4Fe(CN)_6$ that exhibits reversible redox behavior, Fig. 5C, gives a strong photocurrent in the case of *t*-Bu_4PcZn, about a half of that in the presence of HQ. In contrast, the use of $F_{64}PcZn$ shows only negligible photocurrents, 3% of the current in the presence of HQ. The low reactivity of $^1O_2$ towards one-electron donors such as $K_4Fe(CN)_6$ is expected, due to the thermodynamically unfavorable formation of superoxide, since the latter has a lower reduction potential compared to $K_4Fe(CN)_6$.[60, 61] Similar behaviour is observed in the presence of another well-known one-electron donor, ferrocenemethanol, a water-soluble ferrocene derivative with reversible electrochemistry. The photocurrent obtained in

the presence of ferrocenemethanol was 129% of that measured for HQ in the case of *t*-Bu_4PcZn, but only 14% in the case of $F_{64}PcZn$, Table 1.

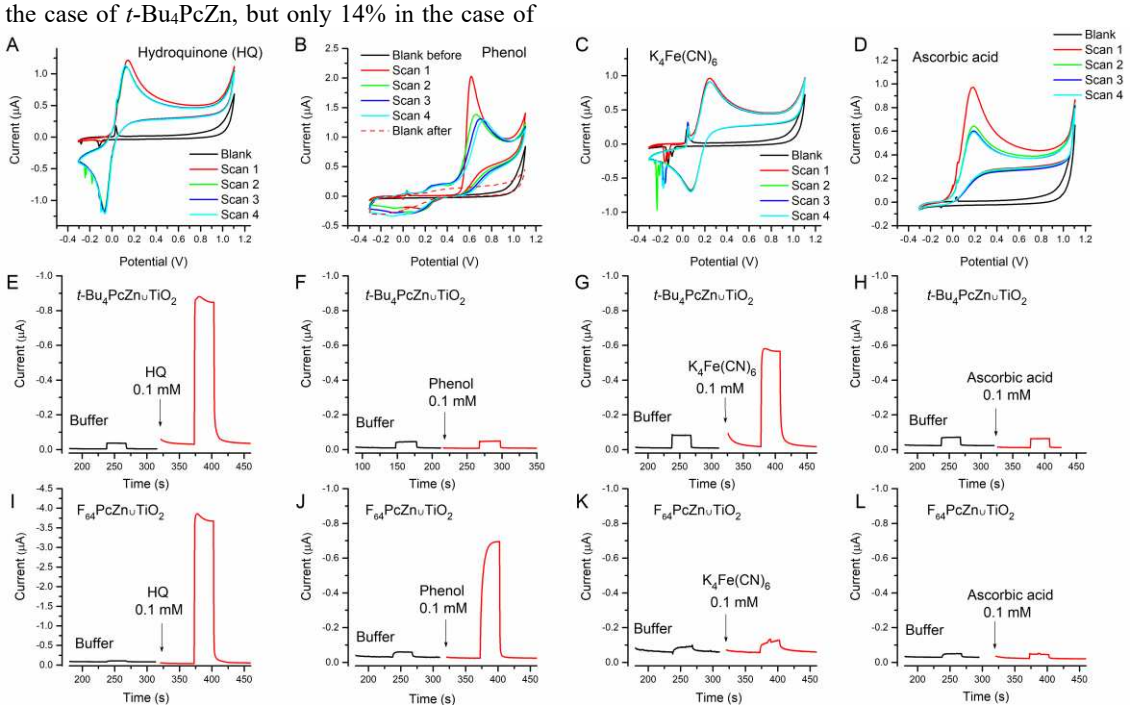

Figure 5. Voltammetric (CV) (panel A-D) and PEC behavior (panel E-L) of four different electron donors. Four consecutive CV scans were conducted to demonstrate repeatability and possible electrode fouling. Broken line in panel B shows an additional CV scan in pure buffer after rinsing the electrode. Scan rate = 0.02 V/s. All potentials are given vs. the Ag-quasi reference (0.040 V vs. SCE, 0.284 V vs. SHE).

To additionally prove that the generation of $^1O_2$ does not result in noticeable photocurrents in the presence of one-electron donors, we tested both *t*-Bu_4PcZn and $F_{64}PcZn$ in methanol solution using the previously reported setup.[48] In the absence of TiO_2, *t*-Bu_4PcZn dissolved in methanol is an efficient $^1O_2$ producing photosensitizer[48, 62], similar to $F_{64}PcZn$.[41, 63] In solutions with the same optical density 0.2 a.u. at the laser wavelength, 659 nm, *t*-Bu_4PcZn and $F_{64}PcZn$ show the same photocurrents (1.0 ± 0.1 μA) in the presence of 1 mM HQ and only negligible photocurrents (0.01 – 0.02 μA) in the presence of 1 mM ferrocenemethanol (Table S3). The results confirm that $^1O_2$ is inefficient in the oxidation of ferrocene, and the comparatively high photocurrents of *t*-Bu_4PcZn on TiO_2 are caused by photoinduced electron transfer reactions.

Finally, ascorbic acid, a well-known one-electron donor with a potential similar to HQ, Fig. 5D, shows no photocurrents for *t*-Bu_4PcZn and $F_{64}PcZn$, Figs. 5H and 5L. Lacking reversibility, ascorbic acid cannot support the redox-cycling mechanism, and thus the electron shuttling between the electrode and the photosensitizer as depicted in Fig. 5D and 2C. This observation also suggests that the photocurrent results from the electron shuttling by the added electron donor, but not from the direct electron transfer mechanisms (Fig. 2A) and not due to secondary ROS such as superoxide that should be formed on TiO_2 as side products of ongoing electron-transfer reactions.

PEC activity of *tert*-butyl-substituted Pcs deposited on TiO_2 materials. Since HQ is an efficient electron shuttle for evaluation of PEC activity of modified TiO_2 materials that exhibit any of the two (Fig. 2B and C) or a mixed oxidation mechanism, HQ was used to discriminate between highly active and poorly active materials, as well as assess the influence of experimental parameters on the activity of the modified electrodes. Fig. 6 shows PEC responses for electrodes coated by TiO_2 PC500 modified by *t*-Bu_4Pcs. The photocurrents in the presence of HQ remarkably exceed the photocurrents in blank buffer and are essentially reproducible in a sequence of at least four illuminations (the decrease in the photocurrent is less than 10%).

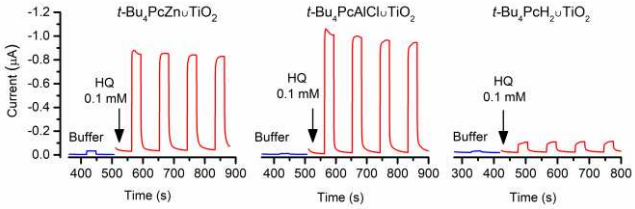

Figure 6. PEC responses of TiO_2 PC500 modified by three different Pcs that inject electrons on CB of TiO_2. Amperometry was conducted in 0.1 M KCl, 0.01 M KH_2PO_4 pH 7 buffer containing 100 μM HQ. Potential applied = −0.2 V.

The other two TiO_2 materials, P25 and P90, showed lower photocurrents compared to PC500, congruent with the TiO_2 specific surface area, Fig. 7. However, the surface area of PC500, see Table S1, is 5x larger compared to P25, but the PEC response is only 2x higher for *t*-$Bu_4PcAlCl$ and 3x higher for *t*-Bu_4PcZn. This can be explained by taking into account the mesoporous structure of PC500 with a significant fraction of pores in the range of 0.5 – 2 nm[64], which can be unavailable for adsorption or blocked by the adsorbed Pc molecules. In general, even for the best configurations, the maximal photocurrents for TiO_2 modified by *tert*-butyl-substituted Pcs are in the range of 0.8 – 0.9 μA (ca. 12 $\mu A \cdot cm^{-2}$), which is 3-4x lower compared to photocurrents obtained with $^1O_2$ generating $F_{64}PcZn$. This difference should be attributed to the faster HQ oxidation kinetics

in the reaction with $^1O_2$ compared to the HQ oxidation via the photoinduced electron transfer.

The influence of the metal centre. Interestingly, *t*-Bu_4PcH_2 shows 10x lower PEC responses compared to *t*-Bu_4PcZn and *t*-$Bu_4PcAlCl$ for all three TiO_2 materials, Fig. 7, although the quantitative deposition of all Pcs was confirmed by leaching them with acetone. The low photocurrent can be explained by a different organization of *t*-Bu_4PcH_2 molecules on the TiO_2 surface due to the weak interaction of *t*-Bu_4PcH_2 with the TiO_2, as discussed above in relation to FTIR data. *t*-Bu_4PcH_2 lacking the metal center that serves as an anchoring point may stay in solution during solvent evaporation until the limited solubility of the Pcs causes its deposition on TiO_2, although likely in aggregated form. Deposition of *t*-Bu_4PcH_2 in the form of multilayers is also expected due to more favorable interaction of CH-rich *t*-Bu_4PcH_2 molecules with each other via van der Waals forces compared to their interaction with hydrophilic OH- and O-rich TiO_2 surfaces. Interestingly, contact angle measurements, Fig. S5, for bare and modified TiO_2 materials showed that intrinsically more hydrophobic *t*-Bu_4PcH_2 (contact angle 157° for *t*-Bu_4PcH_2 and 107° for *t*-Bu_4PcZn) does not insulate hydrophilic TiO_2 surface in contrast to *t*-Bu_4PcZn (contact angle 5° for *t*-Bu_4PcH_2 and 150° for *t*-Bu_4PcZn), which additionally confirms that *t*-Bu_4PcH_2 immobilizes in clusters and does not cover the whole available TiO_2 surface.

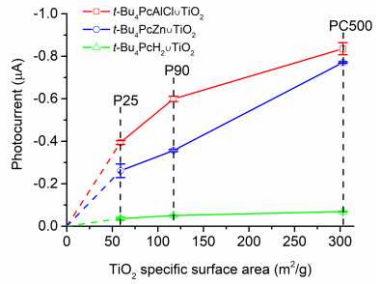

Figure 7. Effect of the TiO_2 specific surface area on the PEC response in the presence of 100 μM HQ.

The role of the metal center was additionally probed by using unsubstituted, planar PcZn, Fig. 1C, which is prone to stacking interaction compared to sterically hindered *t*-Bu_4PcZn. The PEC responses for unsubstituted PcZn are 3x lower compared to *t*-Bu_4PcZn in all three TiO_2 materials, but are still significantly higher (in average by a factor of 3) compared to *t*-Bu_4PcH_2 (Table S4). Thus, the metal center seems to play a crucial role in preserving the PEC activity, likely due to more uniform deposition of Pc on TiO_2 surfaces even when the Pc is prone to aggregation in solution. An electron-deficient $F_{64}PcH_2$, Fig. 1D, which also lacks the metal center to coordinate on TiO_2 surfaces, similarly lost most of the activity observed for $F_{64}PcZn$. The photocurrents do not exceed 10% of that obtained for $F_{64}PcZn$ (Table S4). Similar to *t*-Bu_4PcH_2, the decreased PEC activity of $F_{64}PcH_2$ is attributed to low interaction energy between $F_{64}PcH_2$ and the TiO_2 surfaces leading to likely aggregation and formation of multilayers, which sterically hinder energy transfer to O_2. Also, the $^1O_2$ quantum yield of $F_{64}PcH_2$ in methanol solution is only 0.25 compared to 0.61 for $F_{64}PcZn$[63], which additionally lowers the comparative $F_{64}PcH_2$ activity in our system.

Interestingly, PEC responses in blank buffer were noticeably higher for *t*-Bu_4PcZn (-64 ± 19 nA) compared to *t*-$Bu_4PcAlCl$ (-11 ± 5 nA) and *t*-Bu_4PcH_2 (-10 ± 4 nA). In the absence of other electron acceptors than O_2, this blank photocurrent can be explained by the photocatalytic O_2 reduction via (1) direct electrochemical reduction of photoexcited Pcs, followed by a transfer of the electron to O_2 resulting in $O_2^{\cdot-}$, (2) further reduction of $O_2^{\cdot-}$ and other daughter ROS formed in side reactions. The presence of Cl^- or OH^- as a distal ligand at the metal center of *t*-$Bu_4PcAlCl$ suppresses the blank photocurrent, and thus suggests the role of O_2 or $^1O_2$ coordination in the process.[62]

The effects of the Pc loading on TiO_2 and the thickness of the coatings on electrodes. The optimal performances of the modified TiO_2 materials and the electrode PEC activity depend on the loading of Pc at TiO_2 and the thickness of Pc∪TiO_2 coatings on the electrodes. As expected, the PEC response of *t*-Bu_4PcZn increased when loaded on different TiO_2 materials (expressed in wt%), providing the maximal responses around 800 nA at 3 wt% loadings, Fig. 8A. A similar response is also observed for *t*-$Bu_4PcAlCl$ at 3 wt% loadings on different TiO_2 materials (Fig. S6A). However, the increase of the loading to 5 wt% does not improve the PEC response, likely due to the formation of multilayers. The value of 3 wt% corresponds, on average to 2.6, 5.5, and 13 nm^2 areas per a single Pc molecule for TiO_2 P25, P90, and PC500, respectively. The presence of narrow pores in the range of 0.5-2 nm in PC500[64] that can be unavailable or blocked by adsorbed Pcs may explain the PC500 larger optimal surface area calculated per molecule.

Due to a light-shedding effect, thick electrode coatings by modified TiO_2 can be inefficient. Indeed, varying the amount of Pc∪TiO_2 per electrode surface area in the range from 0.7 to 14 μg·mm^{-2}, which roughly corresponds to thicknesses from 0.2 to 3.3 μm if the layers are uniform, revealed the maximum performance at 11 μg·mm^{-2}, Fig. 8B and Fig. S6B. Below this value the photocurrents increase near linearly with the amount of deposited materials. A thicker Pc∪TiO_2 layer decreases the PEC response by screening the light and reducing the photooxidation efficiency inside the layer at closer distances to the electrode. Thus, the mediated electron exchange current drops due to the larger diffusion distances and correspondingly lower diffusion gradients that define the currents.

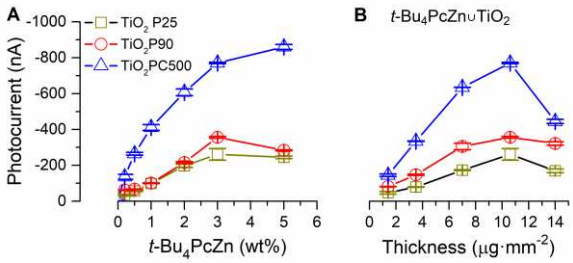

Figure 8. Dependence of the photocurrent; (A) on the loading (wt%) of *t*-Bu_4PcZn immobilized on three different TiO_2 materials. (B) thickness of *t*-Bu_4PcZn deposited on the working electrodes. The measuring buffer contained 100 μM HQ. Potential, -0.25 V. Error bars represent the SD of three independent measurements.

The photocurrent profiles of different phenols. The reversibility of the oxidation/reduction process drives the selectivity of the PEC response of electrodes modified by *t*-Bu_4PcZn/AlCl vs. those modified with $F_{64}PcZn$. Phenol, as discussed above, produces a photocurrent with $^1O_2$-generating $F_{64}PcZn$, but not with *t*-Bu_4PcZn, which requires the reversibility of the electron-transfer process, absent for phenol. The reaction of phenol with

$^1O_2$ leads to the formation of an endoperoxide that rearranges to form BQ.[56-59] Then electrochemical reduction of BQ gives HQ, which is oxidized again by $^1O_2$ to form BQ, thus supporting the mechanism depicted in Fig. 2B.

Given potentially broad analytical applications, the range of tested phenols was extended to include important environmental contaminants and pharmaceuticals bearing the phenolic groups, Table 1. The voltammograms for all used compounds, recorded under conditions identical to those shown in Fig. 5 are presented in Fig. S7. Table 1 summarizes the electrochemical characteristics (reversibility and formal potentials) and the photocurrents measured using TiO_2 modified by electron-rich *t*-Bu_4PcZn/AlCl and the electron-deficient, $^1O_2$ producing F_{64}PcZn.

Importantly, 2,4-dichlorophenol and 2,4,6-trichlorophenol form a new electroactive product under electrochemical oxidation, Fig. S7, resulting in a clear reversible transition at ca. 0 V potential vs. the Ag-quasi reference (0.28-0.29 V vs. SHE), similar to HQ, Table 1. Thus, once oxidized, 2,4-di- and 2,4,6-trichlorophenol can generate photocurrents similarly to HQ. However, the half-peak oxidation potentials are not the same for 2,4-di- and 2,4,6-trichlorophenol (0.795 and 0.759 V vs. SHE, respectively) and lay close to the oxidation potential of *t*-Bu_4PcZn (0.82 V vs. SHE in a non-aggregated state). Thus, the ability of *t*-Bu_4PcZn to oxidize 2,4-dichlorophenol is limited, in agreement with the lower photocurrent, in comparison with 2,4,6-trichlorophenol (Table 1). A higher photocurrent, produced in the case of *t*-Bu_4PcAlCl, is consistent with its 0.28 V higher formal potential vs. *t*-Bu_4PcZn, as measured in solution, Table S2, which should facilitate the oxidation of 2,4-dichlorophenol. Thus, the selection imparted by the energy values of LUMO (the oxidation potential) of the Pcs gives an additional possibility for adjusting the reactivity towards certain electron-shuttling analytes. In contrast, F_{64}PcZn generating $^1O_2$ shows high photocurrents for all chlorinated phenols.

Table 1. Photoelectrochemical responses of analytes at different supported photosensitizers.

Analyte	$E^{0'}$ or $E_{p/2}$ V vs. SHE	Voltammetric reversibility	Photocurrent (μA)[a]		
			t-Bu_4PcZn∪TiO_2	*t*-Bu_4PcAlCl∪TiO_2	F_{64}PcZn∪TiO_2
HQ	0.312	Yes	-0.76 ± 0.03 (100%)	-0.85 ± 0.02 (100%)	-3.03 ± 0.07 (100%)
Phenol	0.854	No	No response	No response	-0.59 ± 0.03 (19%)
$K_4Fe(CN)_6$	0.444	Yes	-0.49 ± 0.01 (64%)	-0.38 ± 0.01 (45%)	-0.09 ± 0.01 (3%)
Ferrocenemethanol	0.477	Yes	-0.98 ± 0.07 (129%)	-0.99 ± 0.02 (116%)	-0.43 ± 0.01 (14%)
L-ascorbic acid	0.364	No	No response	No response	No response
Bisphenol A	0.714	No	No response	-0.013 ± 0.003 (2%)	-1.75 ± 0.08 (58%)
2-Chlorophenol	0.828	No	No response	-0.054 ± 0.005 (6%)	-2.16 ± 0.15 (71%)
3-Chlorophenol	0.909	No	No response	-0.032 ± 0.005 (4%)	-2.84 ± 0.15 (94%)
4-Chlorophenol	0.826	No	No response	-0.023 ± 0.005 (3%)	-1.52 ± 0.08 (50%)
2,4-Dichlorophenol	0.795/0.281[b]	No/Yes[b]	-0.071 ± 0.016 (9%)	-0.165 ± 0.009 (19%)	-2.15 ± 0.15 (71%)
2,4,6-Trichlorophenol	0.759/0.294[b]	No/Yes[b]	-0.306 ± 0.008 (40%)	-0.361 ± 0.012 (43%)	-3.76 ± 0.04 (124%)
Amoxicillin	0.913	No	No response	No response	-0.55 ± 0.03 (18%)
Cefadroxil	0.925	No	-0.04 ± 0.01 (5%)	-0.009 ± 0.003 (1%)	-0.68 ± 0.01 (23%)
Oxytetracycline	0.924	No	No response	-0.017 ± 0.003 (2%)	-0.20 ± 0.01 (7%)
Tetracycline	-	-	No response	No response	-0.16 ± 0.01 (5%)
Paracetamol	0.542	Yes	-0.03 ± 0.01 (4%)	-0.04 ± 0.01 (5%)	-0.10 ± 0.02 (3.4%)

[a]No response = less than 0.02 μA for *t*-Bu_4PcZn∪TiO_2 and less than 0.01 μA for *t*-Bu_4PcAlCl∪TiO_2, in agreement with SD in blanks, which are higher for *t*-Bu_4PcZn∪TiO_2. [b]The second reversible redox process appears after the first scan.

Similar to phenols, the antibiotics amoxicillin, cefadroxil and tetracyclines lack reversibility when oxidized via the electron-transfer pathway, as seen by voltammetry, Fig. S7. This behavior correlates well with the absence of photocurrent when using *t*-Bu_4PcZn/AlCl, Table 1. Nevertheless, the phenolic group in antibiotics is well detectable by F_{64}PcZn, in agreement with our previous works[6, 11], via the singlet oxygen pathway. To confirm that TiO_2 does not play an essential role in the generation of a photocurrent in the presence of amoxicillin, an unmodified electrode and the water-soluble photosensitizer Rose Bengal, known to produce $^1O_2$ in high yields[65] were used. In the presence of 5 μM Rose Bengal, 100 μM amoxicillin gives a photocurrent of -0.14 ± 0.01 μA, which is similar to the -0.11 ± 0.01 μA photocurrent obtained in the presence of 100 μM phenol, but about 10% of the -1.34 ± 0.02 μA photocurrent obtained in the presence of 100 μM HQ (Fig. S8). Thus, $^1O_2$ can transform amoxicillin with an efficacy similar to phenol and generate the corresponding photocurrent without the participation of TiO_2, in agreement with the mechanism in Fig. 2C.

Surprisingly, another drug bearing a phenolic group, paracetamol, produced a comparatively low photocurrent via both pathways (3-5% of the photocurrent for HQ, Table 1) despite its reversible electrochemistry at the bare electrode (Fig. S7). Thus, additional factors, not just reversibility may distinguish between voltammetric behavior and the photosensitized oxidation redox cycling. The photosensitized oxidation of paracetamol, which seems to be impeded due to quenching of photosensitizers by paracetamol or its oxidized derivatives, remains the subject of future investigations.

The effects of $^1O_2$ quenching and O_2 purging from the solution. The addition of NaN_3, a known quencher of $^1O_2$, into the measuring solution suppresses the PEC response of

$F_{64}PcZn \cup TiO_2$ by 50% at 1 mM NaN_3 and 80% at 10 mM NaN_3, Fig. S9. In the case of *t*-$Bu_4PcZn/AlCl \cup TiO_2$, NaN_3 suppresses the PEC responses only by 10% at 1 mM and 20% at 10 mM NaN_3, Fig. S10, corroborating the role of $^1O_2$ for $F_{64}PcZn \cup TiO_2$. However, the NaN_3 quenching effect should be interpreted carefully since NaN_3 is known to quench photosensitizer's triplet states[66], essential for the photoinduced electron transition from Pc to TiO_2. In this view, the photocurrent in the presence of phenol or amoxicillin is a more specific marker for $^1O_2$ generation, whereas the lack of such photocurrent suggests nil $^1O_2$ generation by *t*-$Bu_4PcZn/AlCl \cup TiO_2$.

Notably, the electron-transfer mechanism with redox mediators, Fig. 2C, requires O_2 as an ultimate electron acceptor available in excess and capable of scavenging electrons transferred to the CB of TiO_2. Indeed, the signal drops under Ar purging for 30 min, but recovers after saturation of the measured solution with air, Fig. S11. Similar behavior was previously observed for $F_{64}PcZn \cup TiO_2$,[6] further confirming the essential role of O_2 for both mechanisms (Fig. 2B and C). Noteworthy, previous studies that utilized the direct electron transfer scheme on the electrode (Fig. 2A) were conducted under N_2,[31] i.e., in the absence of O_2, to avoid competition between the underlying electrode and O_2 for the photo-injected electron. This is not of concern in our system, which is thus suitable for broad applications.

CONCLUSIONS

The paradigm of PEC systems based on the photocatalytic conversion of redox mediators that shuttle electrons between photosensitized TiO_2 and an underlying carbon electrode has been demonstrated. The presented methodology can be used for (1) screening the photocatalytic activity of new photosensitizers and related hybrid materials, (2) ascribing the underlying mechanisms to either the $^1O_2$-mediated photooxidation or the photoinduced electron transition, (3) creating PEC sensors. Moreover, the effects of peripheral substituents and the metal center demonstrate the possibility for modulation of photocatalytic reactivity of photosensitized semiconductors and give insights for creating more efficient photocatalysts and more specific PEC sensors.

ASSOCIATED CONTENT

Supporting Information

The Supporting Information is available free of charge on the ACS Publications website.

Supporting information on solid state properties of TiO_2, TLC, FTIR measurements, formal potentials of Pcs, Pcs responses in solution (methanol), water contact angle measurements, voltammetric behavior of phenols, effect of $^1O_2$ quencher and Photocurrent responses in the absence of O_2 (file type, PDF).

AUTHOR INFORMATION

Corresponding Author

* E-mail: karolien.dewael@uantwerpen.be

Author Contributions

The manuscript was written through contributions of all authors.

ACKNOWLEDGMENT

ERA.Net RUS Plus Plasmon Electrolight project (No. 18-53-76006 ERA) is acknowledged by the Belgian and Russian research groups. The work in Belgium was supported by DOCPRO1 project funding from the University of Antwerp and the BOF-SEP project "Diagnostics for Artworks". The work in the US was supported by DTRA (CB10906) and the Center for Functional Materials. M. Marazabadi is thanked for a sample of $F_{64}PcH_2$.

REFERENCES

1. Wang, C.; Li, J.; Mele, G.; Yang, G.-M.; Zhang, F.-X.; Palmisano, L.; Vasapollo, G. *Appl. Catal. B: Environ.*, **2007**, 76, (3), 218-226.
2. Kluson, P.; Drobek, M.; Krejcikova, S.; Krysa, J.; Kalaji, A.; Cajthaml, T.; Rakusan, J. *Appl. Catal. B: Environ.*, **2008**, 80, (3), 321-326.
3. Murphy, S.; Saurel, C.; Morrissey, A.; Tobin, J.; Oelgemöller, M.; Nolan, K. *Appl. Catal. B: Environ.,* **2012**, 119-120, 156-165.
4. Jeon, T. H.; Koo, M. S.; Kim, H.; Choi, W. *ACS Catalysis* **2018**, 8, (12), 11542-11563.
5. Lianos, P. *Appl. Catal. B: Environ.,* **2017**, 210, 235-254.
6. Trashin, S.; Rahemi, V.; Ramji, K.; Neven, L.; Gorun, S. M.; De Wael, K. *Nat. Commun.*, **2017**, 8, (1), 16108.
7. Li, F.; Zhou, Y.; Yin, H.; Ai, S. *Biosens. and Bioelectron.,* **2020**, 166, 112476.
8. Lelii, C.; Bawendi, M. G.; Biagini, P.; Chen, P.-Y.; Crucianelli, M.; D'Arcy, J. M.; De Angelis, F.; Hammond, P. T.; Po, R. *J. Mater. Chem. A*, **2014**, 2, (43), 18375-18382.
9. Urbani, M.; Ragoussi, M.-E.; Nazeeruddin, M. K.; Torres, T. *Coord. Chem. Rev.*, **2019**, 381, 1-64.
10. Yotsumoto Neto, S.; Luz, R. d. C. S.; Damos, F. S. *Electrochem. Commun.,* **2016**, 62, 1-4.
11. Neven, L.; Shanmugam, S. T.; Rahemi, V.; Trashin, S.; Sleegers, N.; Carrión, E. N.; Gorun, S. M.; De Wael, K. *Anal. Chem.*, **2019**, 91, (15), 9962-9969.
12. Haddour, N.; Chauvin, J.; Gondran, C.; Cosnier, S. *J. Am. Chem. Soc.,* **2006**, 128, (30), 9693-9698.
13. Gill, R.; Zayats, M.; Willner, I. *Angew. Chem. Int. Ed.,* **2008**, 47, (40), 7602-25.
14. Hu, Y.; Xue, Z.; He, H.; Ai, R.; Liu, X.; Lu, X. *Biosens. and Bioelectron.,* **2013**, 47, 45-49.
15. Shi, L.; Yin, Y.; Zhang, L.-C.; Wang, S.; Sillanpää, M.; Sun, H. *Appl. Catal. B: Environ.,* **2019**, 248, 405-422.
16. Shu, J.; Tang, D. *Anal. Chem.* **2020**, 92, (1), 363-377.
17. Wang, G.-L.; Liu, K.-L.; Dong, Y.-M.; Wu, X.-M.; Li, Z.-J.; Zhang, C. *Biosens. and Bioelectron.,* **2014**, 62, 66-72.
18. Sivula, K.; van de Krol, R. *Nat. Rev. Mater.,* **2016**, 1, (2), 15010.
19. Bellani, S.; Antognazza, M. R.; Bonaccorso, F. *Adv. Mater.,* **2019**, 31, (9), 1801446.
20. Zada, A.; Muhammad, P.; Ahmad, W.; Hussain, Z.; Ali, S.; Khan, M.; Khan, Q.; Maqbool, M. *Adv. Funct. Mater.,* **2020**, 30, (7), 1906744.
21. Asahi, R.; Morikawa, T.; Irie, H.; Ohwaki, T. *Chem. Rev.,* **2014**, 114, (19), 9824-9852.
22. Guo, Q.; Zhou, C.; Ma, Z.; Yang, X. *Adv. Mat.,* **2019**, 31, (50), 1901997.
23. Asahi, R.; Morikawa, T.; Ohwaki, T.; Aoki, K.; Taga, Y. *Science* **2001**, 293, (5528), 269-271.
24.Won, D.-I.; Lee, J.-S.; Ba, Q.; Cho, Y.-J.; Cheong, H.-Y.; Choi, S.; Kim, C. H.; Son, H.-J.; Pac, C.; Kang, S. O. *ACS Catal.,* **2018**, 8, (2), 1018-1030.
25.Reddy, P. Y.; Giribabu, L.; Lyness, C.; Snaith, H. J.; Vijaykumar, C.; Chandrasekharam, M.; Lakshmikantam, M.; Yum, J. H.; Kalyanasundaram, K.; Grätzel, M.; Nazeeruddin, M. K. *Angew. Chem. Int. Ed.,* **2007**, 46, (3), 373-6.

26. Claessens, C. G.; Hahn, U.; Torres, T. *The Chem. Rec.,* **2008**, 8, (2), 75-97.
27. Mack, J.; Kobayashi, N. *Chem. Rev.,* **2011**, 111, (2), 281-321.
28. Neamţu, M.; Nădejde, C.; Hodoroaba, V. D.; Schneider, R. J.; Panne, U. *Appl. Catal. B: Environ.,* **2018**, 232, 553-561.
29. O'Flaherty, S. M.; Hold, S. V.; Cook, M. J.; Torres, T.; Chen, Y.; Hanack, M.; Blau, W. J. *Adv. Mater.,* **2003**, 15, (1), 19-32.
30.Carrión, E. N.; Loas, A.; Patel, H. H.; Pelmuş, M.; Ramji, K.; Gorun, S. M. *J. of Porphyr. and Phthalocyanines* **2018**, 22, (05), 371-397.
31. Giraudeau, A.; Fan, F.-R. F.; Bard, A. J. *J. Am. Chem. Soc.,* **1980**, 102, (16), 5137-5142.
32. Wang, G.-L.; Xu, J.-J.; Chen, H.-Y.; Fu, S.-Z. *Biosens. and Bioelectron.,* **2009**, 25, (4), 791-796.
33. Hao, Q.; Wang, P.; Ma, X.; Su, M.; Lei, J.; Ju, H. *Electrochem. Commun.,* **2012**, 21, 39-41.
34. Ribeiro, F. W. P.; Moraes, F. C.; Pereira, E. C.; Marken, F.; Mascaro, L. H. *Electrochem. Commun.,* **2015**, 61, 1-4.
35. Blidar, A.; Trashin, S.; Carrión, E. N.; Gorun, S. M.; Cristea, C.; De Wael, K. *ACS Sens.,* **2020**, 5, (11), 3501-3509.
36.Loas, A.; Gerdes, R.; Zhang, Y.; Gorun, S. M. *Dalton Trans.* **2011**, 40, (19), 5162-5.
37. Liao, M. S.; Watts, J. D.; Gorun, S. M.; Scheiner, S.; Huang, M.-J. *J. Theor. Comput. Chem.,* **2008**, 07, (04), 541-563.
38. Gerdes, R.; Lapok, L.; Tsaryova, O.; Wöhrle, D.; Gorun, S. M. *Dalton Trans.,* **2009**, (7), 1098-1100.
39. Moiseeva, E. O.; Trashin, S.; Korostei, Y. S.; Ullah Khan, S.; Kosov, A. D.; De Wael, K.; Dubinina, T. V.; Tomilova, L. G. *Polyhedron,* **2021**, 200, 115136.
40. Lee, H.-J.; Brennessel, W. W.; Lessing, J. A.; Brucker, W. W.; Young, J. V. G.; Gorun, S. M. *Chem. Commun.* **2003**, (13), 1576-1577.
41. Bench, B. A.; Beveridge, A.; Sharman, W. M.; Diebold, G. J.; van Lier, J. E.; Gorun, S. M. *Angew. Chem. Int. Ed.* **2002**, 41, (5), 747-50.
42. S.M. Gorun; R. Gerdes; O. Tsaryova; Lapok, L. *Perfluorophthalocyanine Molecules and Methods of Synthesis.* **2011**.
43. Kobayashi, N.; Ogata, H.; Nonaka, N.; Luk'yanets, E. A. *Chemistry* **2003**, 9, (20), 5123-34.
44. Mizuguchi, J.; Rihs, G.; Karfunkel, H. R. *J. Phys. Chem.,* **1995**, 99, (44), 16217-16227.
45. Alagna, L.; Capobianchi, A.; Casaletto, M. P.; Mattogno, G.; Paoletti, A. M.; Pennesi, G.; Rossi, G. *J. of Mater. Chem.,* **2001**, 11, (7), 1928-1935.
46. Snow, A. W., Phthalocyanine aggregation, The porphyrin handbook. Phthalocyanines: Properties and materials. **2003**; p 129-176.
47. Dhami, S.; Phillips, D. J. *Photochem. Photobiol. A: Chem.,* **1996**, 100, (1), 77-84.
48. Khan, S. U.; Trashin, S. A.; Korostei, Y. S.; Dubinina, T. V.; Tomilova, L. G.; Verbruggen, S. W.; De Wael, K. *ChemPhotoChem* **2020**, 4, (4), 300-306.
49. Diebold, U. Surf. *Sci. Rep.*, **2003**, 48, (5), 53-229.
50.Ou, Z.; Shen, J.; Kadish, K. M. *Inorg. Chem.,* **2006**, 45, (23), 9569-9579.
51. Schöllhorn, B.; Germain, J. P.; Pauly, A.; Maleysson, C.; Blanc, J. P. *Thin Solid Films* **1998**, 326, (1), 245-250.
52.Hesse, K.; Schlettwein, D. *J. Electroanal. Chem.,* **1999**, 476, (2), 148-158.
53. Gouloumis, A.; Liu, S. G.; Sastre, A.; Vazquez, P.; Echegoyen, L.; Torres, T. *Chemistry* **2000**, 6, (19), 3600-7.
54. Ferreira, M.; Varela, H.; Torresi, R. M.; Tremiliosi-Filho, G. *Electrochimica Acta* **2006**, 52, (2), 434-442.
55. Kawde, A.-N.; Morsy, M. A.; Odewunmi, N.; Mahfouz, W. *Electroanal.,* **2013**, 25, (6), 1547-1555.
56. Al-Nu'airat, J.; Dlugogorski, B. Z.; Gao, X.; Zeinali, N.; Skut, J.; Westmoreland, P. R.; Oluwoye, I.; Altarawneh, M. *Phys. Chem. Chem. Phys.,* **2019**, 21, (1), 171-183.
57. Briviba, K.; Devasagayam, T. P. A.; Sies, H.; Steenken, S. *Chem. Res. Toxicol.,* **1993**, 6, (4), 548-553.
58. García, N. A. *J. Photochem. Photobiol. B-Biol.,***1994**, 22, (3), 185-196.
59. Li, C.; Hoffman, M. Z. *J. Phys. Chem. A* **2000**, 104, (25), 5998-6002.
60. Wei, Y.; Wu, K.; Wu, Y.; Hu, S. *Electrochem. Commun.,* **2003**, 5, (9), 819-824.
61. Wood, P. M. *Trends Biochem. Sci.* **1987**, 12, (10), 250-251.
62. Kuznetsova, N. A.; Okunchikov, V. V.; Derkacheva, V. M.; Kaliya, O. L.; Lukyanets, E. A. J. *of Porphy. and Phthalocyanines* **2005**, 09, (06), 393-397.
63. Minnes, R.; Weitman, H.; Lee, H.-J.; Gorun, S. M.; Ehrenberg, B. *Photochem. Photobiol.,* **2006**, 82, (2), 593-599.
64. Ribbens, S.; Beyers, E.; Schellens, K.; Mertens, M.; Ke, X.; Bals, S.; Van Tendeloo, G.; Meynen, V.; Cool, P. *Microporous and Mesoporous Mater.,* **2012**, 156, 62-72.
65.Wilkinson, F.; Helman, W. P.; Ross, A. *J. Phys. Chem. Ref. Data,* **1993**, 22, 113-262.
66. Harbour, J. R.; Issler, S. L.; Hair, M. L. *J. Am. Chem. Soc.,* **1980**, 102, (26), 7778-7779.